Modeling of AZ31 Magnesium Alloy Fracture under Dynamic Loading Using a Failure Model of Active Type

Sergey A. Zelepugin[1, 2, a)], Vladimir V. Skripnyak[1, b)], Vladimir A. Skripnyak[1, c)] and Alexander E. Kiryushkin[1, d)]

[1]*National Research Tomsk State University, 36 Lenin Avenue, Tomsk, Russia, 634050*
[2]*Tomsk Scientific Centre SB RAS, 10/4 Akademicheskii Avenue, Tomsk, Russia, 634055*

[a)] Corresponding author: szel@yandex.ru
[b)] skrp2012@yandex.ru
[c)] skrp2006@yandex.ru
[d)] sashakir94@mail.ru

Abstract. A kinetic fracture model of active type is presented, and model constants are selected to describe spall fracture in AZ31 magnesium alloy under shock-wave loading. The specific volume of microdamage is used as a damage parameter. This parameter, which is part of the total volume of the medium, is included in the governing equations and continuously modifies the material properties, causing stress relaxation. Numerical calculations of the impact of an aluminum plate on a cylindrical specimen made of AZ31 magnesium alloy at an initial impact velocity of 660 m/s are performed in a two-dimensional axisymmetric statement. The formation of a spall plate in the AZ31 magnesium alloy specimen is demonstrated when tensile stresses exceed a critical value of ~0.3 GPa. The calculation results are compared with experimental data, and qualitative and quantitative agreement is obtained.

INTRODUCTION

Currently, one of the pressing issues is the study of the behavior of magnesium alloys under quasi-static and dynamic loading [1–3]. Magnesium alloys receive such attention due to their excellent mechanical properties (low density, high specific strength, etc.), resulting in their use in aerospace and automotive engineering, computer technology, etc.

An important task is to evaluate the deformation and fracture characteristics of magnesium alloys under dynamic loading. It is important to select optimal parameters for the governing equations, including the Johnson-Cook, Zerilli-Armstrong, and other models [4–7]. It is also necessary to develop fracture models for magnesium alloys under shock-wave loading [8–11].

The goal of this study is to substantiate the applicability of the kinetic fracture model of active type [12] for describing spall fracture in an AZ31 magnesium alloy specimen and to select the constants for this model.

PROBLEM STATEMENT

This paper numerically simulates the impact of an aluminum plate with a cylindrical specimen made of AZ31 magnesium alloy. The impact conditions correspond to those of experiment [9]. The diameter of the impact plate is 40 mm, and the plate thickness is 0.85 mm. The diameter of the cylindrical specimen is also 40 mm, and the specimen height is 4.97 mm. The initial impact velocity is chosen to be 660 m/s.

This problem is characterized by the presence of an axis of symmetry, so the simulation is performed in a two-dimensional axisymmetric setting.

The general system of equations describes the unsteady adiabatic motion of an elastic-plastic medium using a model of a damaged medium. In this model, the volume of a medium element consists of the volume of the undamaged

portion and the volume of microdamage, with microdamage uniformly distributed throughout the volume of the medium. The average density of the damaged medium is adjusted to account for the volume of microdamage.

The general system of equations includes the equations of continuity, motion, and energy [13, 14]. The equation of state determining the pressure in the undamaged portion of the medium is chosen in the Mie-Grüneisen form. A method for determining the equation of state parameters using the Hugoniot shock adiabatic constants is employed. Plastic flow is modeled using the von Mises yield condition.

To simulate the initiation and evolution of microdamage, a kinetic model of active fracture is used [12]. In this model, the rate of change in the specific volume of microdamage is determined by the equations:

$$\frac{dV_f}{dt} = \begin{cases} 0, if\ |P_c| \le P^*\ or\ (P_c > P^*\ and\ V_f = 0) \\ -sign(P_c)K_f(|P_c| - P^*)(V_2 + V_f), \\ if\ P_c < -P^*\ or\ (P_c > P^*\ and\ V_f > 0) \end{cases} \quad (1)$$

$$P^* = P_k V_1/(V_f + V_1). \quad (2)$$

Here, V_f is the specific volume of microdamage, Pc is the pressure in the undamaged component of the medium, and V_1, V_2, P_k, and K_f are model constants. The constants in (1, 2) were selected by comparing the results of calculations and experiments recording the free surface velocity when loading the specimen with plane compression pulses. The same set of material constants can be used to calculate both the growth and collapse of microdamage, depending on the sign of P.

When constructing model (1), it was assumed that the material contains potential fracture nucleus of identical initial sizes with an effective specific volume V_1, on which cracks or pores form and grow when the tensile pressure exceeds the critical value P^*, which decreases as the resulting microdamage grows. A typical change in the critical value P^* as a function of the specific volume of microdamage V_f is shown in Fig. 1. In this case, the parameters V_1 and P_k had the following values: $V_1 = 2.5\ 10^{-6}$ m^3/kg, $P_k = 1.5$ GPa.

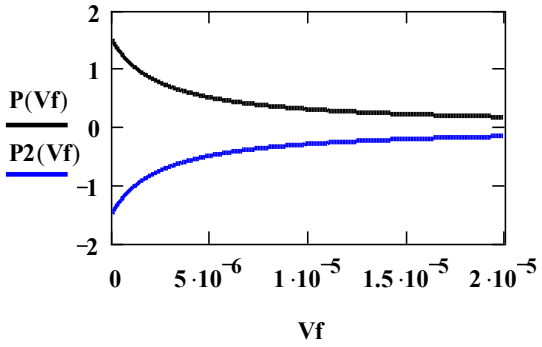

FIGURE 1. A typical change in the critical value P^* (2) as a function of the specific volume of microdamage.

The lower curve P2(Vf) in Fig. 1 demonstrates the change in the critical value of P^* under tensile pressures. Microdamage initiation in an initially undamaged medium occurs when the tensile pressure exceeds P_k (in this case, -1.5 GPa). As the specific volume of microdamage increases, the critical value of P^* decreases, facilitating the failure of the material. When the pressure reverses sign, the change in the critical value of P^* is characterized by the upper curve, which shows an increase in P^* with decreasing V_f. In the region between the curves, no change in the specific volume of microdamage (either increase or decrease) occurs.

The value of V_1 for a material without initial porosity is set within the range of 0.2–2.0%, on average 1% or $0.01V_0$, where V_0 is the initial relative volume, a quantity inversely proportional to the material density. The value of V_2 is selected from the interval of $0.00001V_0 < V_2 < V_1$. Constants V_3, V_4 are choses in the interval of 10–40% of the initial relative volume. Quantity P_k is selected in the interval of $S_k < P_k < \sigma_{sp}$, where S_k is the true quasistatic tensile stress, σ_{sp} is the material spallation strength, determined from the experiments on collision of plates. Constant K_f is selected in the interval of (0.1–0.01) 1/(GPa·s).

The spall fracture of the AZ31 magnesium alloy is described using the following coefficients of the fracture model: $V_1 = 8.38 \cdot 10^{-3}$ cm^3/g, $V_2 = 5.59 \cdot 10^{-4}$ cm^3/g, $V_3 = 0.03$ cm^3/g, $V_4 = 0.2$ cm^3/g, $K_f = 0.007$ (m·s)/kg, $P_k = -0.3$ GPa.

Other constants characterizing aluminum and magnesium alloy AZ31 can be found in [8].

This paper uses dependences of material strength properties on the specific volume of microdamage. Equations (3) present the dependences for the yield strength and shear modulus, and Fig. 2 shows a typical form of such dependences. The yield strength for ductile metals and alloys decreases linearly with increasing material damage level up to a critical value of the specific volume of microdamage (constant V_4), after which the material is considered to be destroyed, and the yield strength becomes zero. The shear modulus changes relatively little with increasing material damage.

$$G = G_0 \frac{V_3}{(V_f + V_3)} \qquad \sigma = \begin{cases} \sigma_0 \left(1 - \frac{V_f}{V_4}\right), if\ V_f \le V_4 \\ 0, if\ V_f > V_4 \end{cases} \tag{3}$$

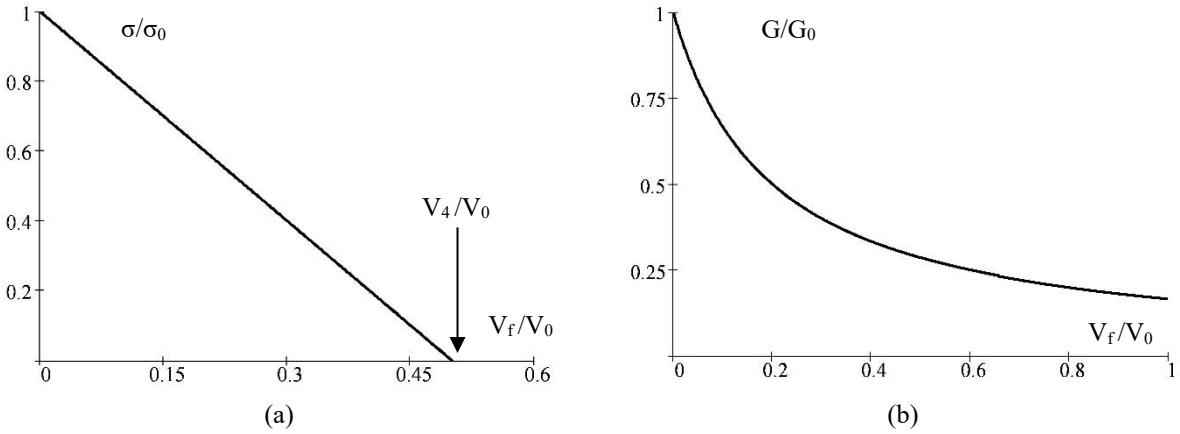

FIGURE 2. Typical dependences of yield strength (a) and shear modulus (b) on the specific volume of microdamage.

The problem was solved using a modified finite element method [13]. This FEM modification was developed by G. Johnson [15] and involves implementing the principle of local action at the computational time step for high-speed processes, eliminating the need for a global stiffness matrix. The research computer code COMP2, developed by the first author of this paper, was used for numerical modeling.

RESULTS AND DISCUSSION

Figure 3 illustrates the dynamics of shock wave propagation (Fig. 3a) and the initiation and development of microdamage regions (Fig. 3b) in the specimen and impactor. Axes are in mm.

Figure 3a shows the change in pressure fields and contours at successive time instants of 0.1, 0.8, and 1.3 μs (from top to bottom, respectively) in the radial cross-section of the interacting bodies. For the time instant of 0.1 μs, the range from 0 to 5.2 GPa was selected with an interval of 0.3 GPa. The results demonstrate the propagation of plane shock fronts along the impactor-plate and the target-specimen. Shock front unloading is observed on the free lateral surface. However, a significant portion of the shock front remains plane, confirming the applicability of the one-dimensional analytical estimates given in [9], at least up to a certain point in the impact process.

Middle fragment of Fig. 3a corresponds to a time moment of 0.8 μs. The pressure range for this time moment was chosen from -0.25 to 1.86 GPa with an interval of 0.1 GPa. By this time, the shock front has moved to the center of the specimen. As it propagates, the pressure amplitude in the shock wave decreases. Also, due to unloading waves from the side surface of the specimen and the rear surface of the impactor, the shock front length is reduced. A distinctive feature of this moment in the process is the appearance of negative (tensile) pressures. In these areas, according to the active fracture model (1, 2), microdamage zones can initiate and grow.

The lower fragment of Fig. 3a corresponds to a time of 1.3 μs. The pressure range for this time was chosen from -0.39 to 0.34 GPa with an interval of 0.02 GPa. The pressure amplitude has dropped significantly by this time. A characteristic feature of the process at this point in time is the formation of a region of negative pressure along the sample's radius, approximately one-third of the sample's height from its rear surface. In this region, rear spalling is possible. A region of negative pressure near the side surface of the sample has also developed significantly, extending from the front to the rear surfaces, encompassing the entire height of the sample.

Figure 3b shows the change in the fields and contours of the specific microdamage volume at successive time instants of 1, 1.5, and 2 μs (from top to bottom, respectively) in the radial cross-section of the interacting bodies. The range of variation for this parameter was chosen to be common for all presented time instants and was 0–0.04 cm^3/g with an interval of 0.005 cm^3/g.

The calculation results for the time instant of 1 μs (the upper fragment of Fig. 3b) demonstrate the initiation of microdamage regions near the lateral surface, with these regions forming in both the specimen and the impactor. The middle fragment of Fig. 3b, corresponding to the time instant of 1.5 μs, shows the formation of spall fracture along the specimen radius. Moreover, the rear spall region is aligned with the fracture regions near the lateral surface of the specimen.

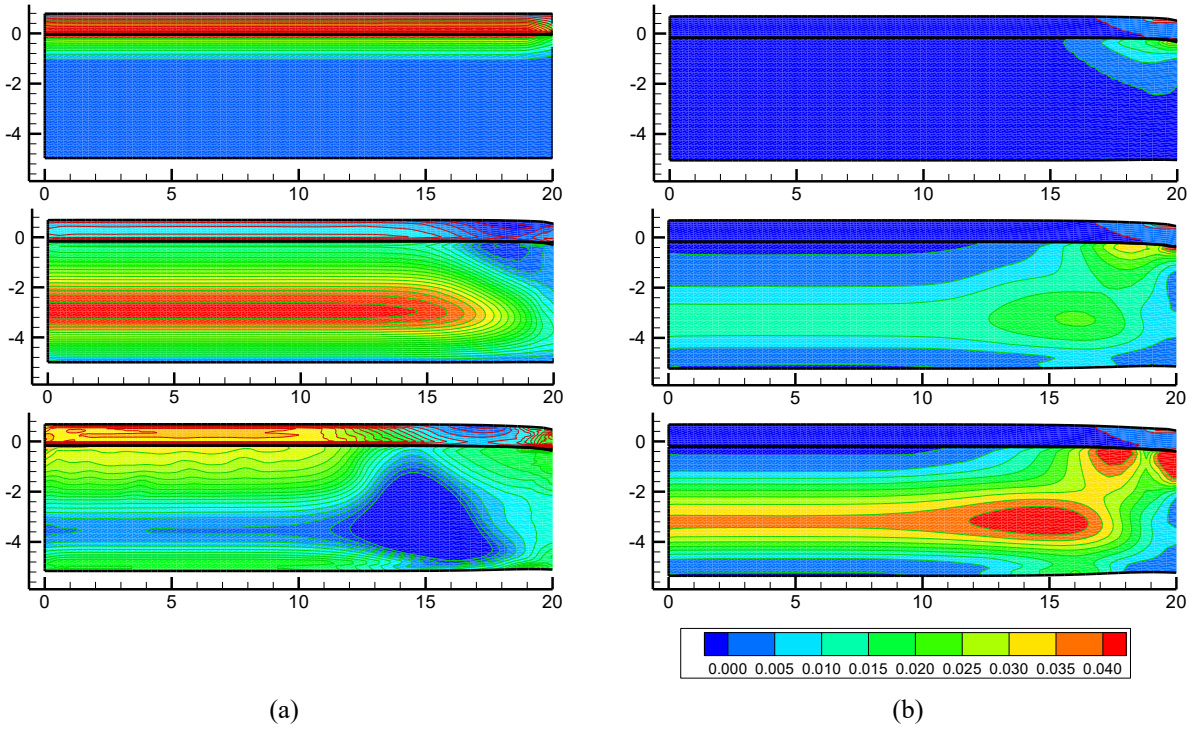

FIGURE 3. Fields and contours of process parameters in the sample: (a) pressure, (b) specific volume of microdamage.

The lower fragment of Fig. 3b, corresponding to a time of 2 μs, demonstrates the development of both the rear spall fracture and the fracture areas near the side surface. The shape of the microdamage areas at a time of 2 μs indicates the formation of a spall plate with a radius of approximately 2/3 of the specimen radius and a thickness of approximately 2.2 mm.

Another characteristic feature of this process is the absence of development of microdamage in the impactor at the stage of influence of shock and reflected waves. This indicates that the impactor fails via a different mechanism associated with plastic deformation.

CONCLUSION

The research results presented in this article demonstrate that the active-type kinetic fracture model can be successfully applied to describe spall fracture in the AZ31 magnesium alloy specimen under shock-wave loading.

The constants for this model are selected, the methodology for their selection is described, and it is determined that the damage in the AZ31 polycrystalline alloy, starting nucleation upon the development of tensile stresses, is equal to 0.3 GPa.

ACKNOWLEDGMENTS

The research was supported by the Russian Science Foundation (grant no. 24-79-10103, https://rscf.ru/project/24-79-10103/). The authors thank the Russian Science Foundation for the support.

REFERENCES

1. L. Zhang, Q. Yuan, J. Tanm, Q. Dong, H. Lv, F. Wang, A. Tang, J. Eckert, and F. Pan, Enhancing the room-temperature plasticity of magnesium alloys: Mechanisms and strategies. *Journal of Magnesium and Alloys* **12**(12), 4741–4767 (2024). https://doi.org/10.1016/j.jma.2024.12.008
2. E. Tur and F. Öztürk, AZ31 magnesium alloy in the aerospace industry: A review on the effect of composition, microstructure, and mechanical properties on alloy performance. *Kocaeli Journal of Science and Engineering* **7**(2), 109–130 (2024). https://doi.org/10.34088/kojose.1334496
3. V. V. Skripnyak and V. A. Skripnyak, Hexagonal close-packed (hcp) alloys under dynamic impacts. *Journal of Applied Physics* **131**, 165902 (2022). https://doi.org/10.1063/5.0085338
4. F. Zhang, Z. Liu, Y. Wang, P. Mao, X. Kuang, Z. Zhang, Y. Ju, and X. Xu, The modified temperature term on Johnson-Cook constitutive model of AZ31 magnesium alloy with {0002}. *Journal of Magnesium and Alloys* **8**(1), 172–183 (2020). https://doi.org/10.1016/j.jma.2019.05.013
5. S. A. Zelepugin, R. O. Cherepanov, and N. V. Pakhnutova, Optimization of Johnson–Cook constitutive model parameters using the Nesterov gradient-descent method. *Materials*, **16**, 5452. (2023). https://doi.org/10.3390/ma16155452
6. V. A. Skripnyak, M. O. Chirkov, and V. V. Skripnyak, Mechanical behavior of aluminum alloy 1520 under tension in the range of strain rates from 10^{-1} to 10^{3} s^{-1}. Vestnik TSU. Math. Mech. **86**. 120–135. (2023). https://doi.org/10.17223/19988621/86/9
7. V. V. Skripnyak and V. A. Skripnyak, Mechanical behavior of titanium alloys in a mechanical punch test. Vestnik TSU. Math. Mech. **89**, 147–161 (2024). https://doi.org/10.17223/19988621/89/11
8. S. A. Zelepugin, V. V. Skripnyak, V. A. Skripnyak, and A. E. Kirushkin, Fracture model of an AZ31 magnesium alloy under dynamic loading. *Russ Phys J.*, **68**, 229–236 (2025). https://doi.org/10.1007/s11182-025-03423-1
9. G. V. Garkushin, G. I. Kanel', and S. V. Razorenov, High strain rate deformation and fracture of the magnesium alloy Ma2-1 under shock wave loading. *Physics of the Solid State* **54**, 1079–1085 (2012). https://doi.org/10.1134/S1063783412050101
10. D. D. Mallick, S. E. Prameela, D. Ozturk, C. L. Williams, M. Kang, G. M. Valentino, J. T. Lloyd, J. W. Wilkerson, T. P. Weihs, and K. T. Ramesh, Spall strength in alloyed magnesium: A compendium of research efforts from the CMEDE 10-year effort. *Mechanics of Materials* **162** 104065 (2021). https://doi.org/10.1016/j.mechmat.2021.104065
11. S. Ashitkov, P. Komarov, S. Romashevskiy, E. Struleva, and S. Evlashin, Shock compression of magnesium alloy by ultrashort loads driven by sub-picosecond laser pulses. *Journal of Applied Physics* **132**, 175104 (2022). https://doi.org/10.1063/5.0082476
12. G. I. Kanel and V. V. Sherban, Plastic deformation and spall fracture of Armco iron in a shock wave. *Combustion, Explosion, and Shock Waves*, **16**(4), 93–103 (1980).
13. V. A. Gorelski, S. A. Zelepugin, and A. Yu. Smolin, Effect of discretization in calculating three-dimensional problems of high-velocity impact by the finite-element method. *Computational Mathematics and Mathematical Physics*, **37**(6), 722–730 (1997).
14. V. A. Gorel'skii, S. A. Zelepugin, and V. N. Sidorov, Numerical solution of three-dimensional problem of high-speed interaction of a cylinder with a rigid barrier, taking into account thermal effects. *International Applied Mechanics* **30**(3), 193–198 (1994). https://doi.org/10.1007/BF00847334
15. G. R. Johnson, Numerical algorithms and material models for high-velocity impact computations. *International Journal of Impact Engineering* **38**, 456–472 (2011). https://doi.org/10.1016/j.ijimpeng.2010.10.017